Nanomedicine: Nanotechnology, Biology, and Medicine
15 (2019) 86 – 97

nanomedjournal.com

Galactosylated chitosan triptolide nanoparticles for overcoming hepatocellular carcinoma: Enhanced therapeutic efficacy, low toxicity, and validated network regulatory mechanisms

Yan-Qiong Zhang, PhD[a,1], Yan Shen, PhD[b,1], Ming-Mei Liao, MD[c], Xia Mao, MS[a], Gu-Jie Mi, PhD[d], Chen You, MS[e], Qiu-Yan Guo, PhD[a], Wei-Jie Li, BS[a], Xiao-Yue Wang, BS[a], Na Lin, PhD[a,*], Thomas J. Webster, PhD[d,*]

[a]*Institute of Chinese Materials Medical, China Academy of Chinese Medical Sciences, Beijing, China*
[b]*Department of Pharmaceutics, China Pharmaceutical University, Nanjing, China*
[c]*Key Laboratory of Nanobiological Technology of Chinese Ministry of Health, Xiangya Hospital, Central South University, Changsha, Hunan, China*
[d]*Department of Chemical Engineering, Northeastern University, Boston, USA*
[e]*Jiangsu Provincial Xuzhou Pharmaceutical Vocational College, Xuzhou, China*

Received 11 July 2018; accepted 3 September 2018

Abstract

Hepatocellular carcinoma (HCC) is the second leading cause of cancer-related deaths worldwide. Current therapies present significant limitations. Triptolide (TP) is highly effective against multiple cancers including HCC. However, high toxicity, low water solubility, and unknown therapeutic targets limit its clinical application. Herein, we designed galactosylated-chitosan-TP-nanoparticles (GC-TP-NPs) with high drug loading capacities for targeted delivery to HCC. In addition to a sustained release pattern, an efficient asialoglycoprotein receptor mediated cellular uptake *in vitro*, and high liver tumor accumulation *in vivo*, GC-TP-NPs showed lower systemic and male reproductive toxicities than free TP. Importantly, GC-TP-NPs retained the anti-cancer activities of the free TP, exerting the same pro-apoptotic and anti-proliferative effects on HCC cells *in vitro*, and displayed higher efficacies in reducing tumor sizes *in vivo*. Further investigation revealed that GC-TP-NPs induced cancer cell apoptosis via blocking TNF/NF-κB/BCL2 signaling. Collectively, GC-TP-NP represents a promising candidate in halting liver cancer progression while minimizing systemic toxicity.

Key words: Triptolide; Nanoparticle; Hepatocellular carcinoma; Network pharmacology; Toxicity

Hepatocellular carcinoma (HCC) is the most common type of liver cancer and the second leading cause of cancer-related deaths worldwide.[1] Specifically, nearly half of new HCC diagnoses occur in China.[2] Current therapeutic strategies, including surgery, transarterial embolization, chemoembolization, targeted drug therapy, biotherapy, traditional Chinese medicine (TCM), and liver transplantation, have been extensively used in the treatment of HCC.[3] Nonetheless, these methods present several significant limitations.[4] Due to the lack of target selectivity, conventional systemic chemotherapies are often associated with a high risk of recurrence, multi-drug resistance, and serious side effects.[5,6] Therefore, it is of great clinical significance to develop novel and efficient therapeutic strategies against HCC.

Triptolide (TP), an active component derived from the Chinese herb *Tripterygium wilfordii* Hook F (TwHF), has been used to treat inflammation and autoimmune diseases for

Funding: This study was supported by the National Natural Science Foundation of China (No. 81673834), Beijing Nova Program (No. Z1511000003150126), the Fundamental Research Funds for the Central Public Welfare Research Institutes (No. Z2017082 & L2017018).

Conflicts of interest: The authors do not have any conflicts of interest with the content of the manuscript.

*Corresponding authors.
E-mail addresses: nlin@icmm.ac.cn, (N. Lin), th.webster@neu.edu. (T.J. Webster).

[1] These authors contributed equally to this study.

https://doi.org/10.1016/j.nano.2018.09.002
1549-9634/

centuries.[7,8] Accumulating evidence suggests that TP may possess anti-inflammatory and anti-cancer effects.[9] For instance, a previous study demonstrated that TP inhibited the growth of multiple cancer cells, including both hematologic malignancies and solid tumor cells, at low concentrations, supporting its use as an effective chemotherapeutic agent.[10] However, the clinical application of TP is limited due to its high toxicity and low water solubility.[11] To address this problem, a recent study synthesized a prodrug of TP, named Minnelide™, that showed greater water solubility and contained a site for rapid de-phosphorylation. Despite the improved solubility and extended serum half-life, the inability to target cancer cells has limited its anti-cancer efficacy.[12] Thus, there is an urgent need to develop a cancer targeted drug delivery system for TP.

Nanomedicine-based targeted drug delivery systems deliver drugs to specific organs or tissues using nanoscale particles.[13] These systems are characterized by simple preparation, high drug loading capacity, excellent stability, improved drug accumulation, and reduced toxicity,[14] which make them extremely promising anti-cancer agents. Extensive studies have shown that nanoparticles (NPs) can enter neoplastic sites through both active and passive targeted deliveries. Active targeting commonly utilizes ligand-receptor interactions while passive targeting takes advantage of the enhanced permeability and retention (EPR) effect for preferential tumor accumulation of NPs.[15,16] With regard to hepatocyte-targeted delivery systems, an increasing number of studies have used galactosylated polymers to prepare NPs for the active targeted delivery of anti-cancer drugs based on the hypothesis that asialoglycoprotein receptors (ASGP-R) on liver cancer cells can bind to ligands containing specific terminals such as β-D-galactose and N-acetylgalactosamine residues.[17,18] Chitosan (CS), a nontoxic and biodegradable polycationic polymer, is considered as an excellent carrier with high biocompatibility, excellent biodegradability, and low toxicity.[19] It has been reported in recent studies that several galactosylated CS derivatives appear to be hepatocyte-specific carriers,[20–22] suggesting their targeting potential.

In this study, we prepared galactosylated-CS(GC)-TP-NPs (GC-TP-NPs) for HCC targeted therapy and systematically evaluated their physicochemical properties, drug release profiles, as well as cellular uptake, biodistribution and anti-tumor efficacies. In addition, hepatic, renal and male reproductive toxicities were also extensively characterized *in vivo* to evaluate their safety. Finally, we performed a network pharmacology-based investigation with the attempt to decipher molecular mechanisms of GC-TP-NP targeted drug delivery (Supplementary Figure S1).

Methods

Ethics statement

All experimental protocols were approved by the Research Ethics Committee of the China Academy of Chinese Medical Sciences (approval number: 2016-030-SQ). Animal experiments were carried out in accordance with the guidelines and regulations for the care and use of laboratory animals of the Center for Laboratory Animal Care.

Preparation and characterization of the GC-TP-NPs

GC-TP-NPs were prepared by using the tripolyphosphate cross-linking method following the protocols described in Supplementary File S1-section 1. The degree of substitution of galactose residues [DSGC (%)] in GC was estimated by ^{1}H NMR and was calculated using the Eq. f1[23]:

$$DS_{GC} = \frac{H_{GC(\delta 3.3-4.2)} - H_{CS(\delta 3.5-4.0)}}{12} \times 100\% \quad \text{f1}$$

Where $H_{GC(\delta 3.3\text{-}4.2)}$ was the amount of hydrogen atoms of GC at δ 3.3-4.2 ppm and $H_{CS(\delta 3.3\text{-}4.2)}$ was the amount of hydrogen atoms of CS at δ 3.3-4.2 ppm.

The mean size, size distribution and zeta potential of the GC-TP-NPs were measured by a Malvern Mastersizer 2000 particle size analyzer (Zetasizer Nano ZS90, Malvern Instruments Ltd, UK). The morphology of the GC-TP-NPs was examined by transmission electron microscopy (TEM, JEM-2100, JEOL, Japan). Loading efficiency (LE) and encapsulation efficiency (EE) of the GC-TP-NPs were determined spectrophotometrically, and were calculated by Eqs. f2 and f3, respectively:

$$LE(\%) = \frac{Me}{Mn} \times 100\% \quad \text{f2}$$

$$EE(\%) = \frac{Me}{Mt} \times 100\% \quad \text{f3}$$

where Me is the mass of TP encapsulated inside the GC-TP-NPs; Mn is the mass of the GC-TP-NPs; and Mt is the total mass of TP used in the preparation of the GC-TP-NPs.

The release profile of TP from GC-TP-NPs *in vitro* was evaluated as described in Supplementary File S1-section 2.

ASGP-R mediated cellular uptake of GC-NPs

A comparative cellular uptake study of the free TP, CS-TP-NPs and GC-TP-NPs was carried out on a human HCC cell line SMMC-7721 and an adenocarcinoma human alveolar basal epithelial cell line A549 (Cat No.3111C0001CCC000087 and Cat No.3111C0001CCC000002, respectively, Cell Bank of the Chinese Academy of Medical Science, Beijing, China) as described in Supplementary File S1-section 3.

In vivo fluorescence imaging for NPs biodistribution

To determine the biodistribution of the GC-NPs *in vivo*, DIR-780 (KeyGEN BioTECH, China) was used to replace TP during NP preparation and the human HCC cell line SMMC-7721 tumor-bearing nude mouse model was established. The detailed protocols are provided in Supplementary File S1-section 4.

Toxicity evaluation

Hepatic and renal toxicities

To evaluate the hepatic and renal toxicities of the GC-TP-NPs, 30 male Kunming mice (4-6 weeks of age and 25±2 g of weight, Charles River Laboratories, production license No: SCXK 2012-0001, MA, USA) were randomly divided into five groups (5 mice per group) and were administrated

intragastrically with 1 mg/kg TP (TP-low group), 2.5 mg/kg TP (TP-high group), 6.76 mg/kg GC-TP-NPs (GC-TP-NP-low group), 16.90 mg/kg GC-TP-NPs (GC-TP-NP-high group) and PBS (control group) once daily for 6 weeks. Mice were sacrificed the next day after the last administration. Liver and kidney tissues were dissected from each group and weighed using an electronic balance (Satorius, Goettingen, Germany). The liver and kidney indexes were calculated by Eq. f4:

$$\text{Liver/kidney/testis/epididymis idexes} = \frac{\text{Mass of Liver/kidney/testis/epididymis(g)}}{\text{Body weight(g)}} \times 100\% \quad \text{f4}$$

In addition, the serum levels of liver and kidney injury markers, including alanine aminotransferase (ALT, for liver), aspartate transaminase (AST, for liver), urine creatinine (Cr, for kidney) and blood urea nitrogen (BUN, for kidney), were detected using standardized kinetic and fixed-rate colorimetric procedures.

Moreover, the paraformaldehyde-fixed liver and kidney tissues were embedded in paraffin and sectioned at a thickness of 4 μm. Hematoxylin and eosin (H&E) staining was performed and the stained sections were observed under an optical microscope (Carl Zeiss AG, Jena, Germany). All sections were assessed by two experienced observers who were blinded to the background of this study.

Male reproductive toxicity

To evaluate the male reproductive toxicity of the GC-TP-NPs, the testis and epididymis indexes were calculated by Eq. f4. The serum levels of testosterone (Cat. No. DRE30439, BIO-SWAMP), glutathione peroxidase (GSH-PX, Cat. No. DRE30907, BIO-SWAMP) and α-glucosidase (Cat. No. DRE30215, BIO-SWAMP) were detected by enzyme linked immunosorbent assays (ELISA) using commercially available kits (Beijing Lvyuan Bode Biotechnology Inc., Beijing, China). Histopathology of the testis and epididymis tissues obtained was also assessed by H&E staining using a previously described method. Finally, sperm characteristics, including epididymal sperm count, density, motility and viability, were measured by the TOX IVOS Sperm analyzer (Hamilton Thorne Research, Beverly, MA).

In vitro and in vivo anti-tumor activity

The anti-HCC activities of the GC-TP-NPs *in vitro and in vivo* were evaluated as described in Supplementary File S1-section 5-6.

Identification of network targets of TP against HCC

Prediction of TP putative targets

TP putative targets were predicted using MedChem Studio (version 3.0; Simulations Plus, Inc., Lancaster, CA, USA, 2012) through a structural similarity search. The component-putative targets that have similarity scores higher than 0.85 (high similarity) were selected for further investigation. The list of TP putative targets is provided in Supplementary Table S1.

Network construction and analysis

HCC-related genes (Supplementary Table S2) were identified in our previous studies.[24,25] The drug target-disease gene network was constructed using links between TP putative targets and HCC-related genes according to the public database STRING (http://string-db.org/, version 10.0). The networks were visualized by Navigator software (Version 2.2.1).

Pathway enrichment analyses

Pathway enrichment analysis of TP candidate targets against HCC was performed using DAVID (http://david.abcc.ncifcrf.gov/home.jsp, version 6.7) based on the data obtained from the KEGG database (http://www.genome.jp/kegg/, Last updated: Oct 16, 2012). Only KEGG pathways with P values less than 0.05 (corrected using the Bonferroni method) were selected.

Western blot analysis

Western blot analysis was performed to analyze protein expression levels of 6 TP candidate targets against HCC, including TNF, NFKB1, NFKB1A, RELA, BCL2 and XIAP, in liver tumor tissues following a procedure previously described.[26,27] A list of antibodies used is provided in Supplementary Table S3.

Statistical analysis

SPSS statistical software (Version 11.0) was used to perform the statistical analysis in this study. All experiments were repeated three times. Data are represented as mean±S.D. Differences among experimental groups were determined by Student's t-test. P values less than 0.05 was considered as statistically significant.

Results

Characterization of the GC-TP-NPs

As the study was directed towards achieving a CS derivative targeted to hepatocytes, ligand modification of the CS was carried out with lactobionic acid to incorporate galactose groups into the CS backbone using a tripolyphosphate cross-linking method. CS has a pKa value of about 6.2-7.0, so it is only soluble in an acidic environment. CS is readily soluble in acid aqueous solutions (pH 4.5-6.5) due to protonation of the amino group: $-NH_2 + H^+ \leftrightarrow -NH_3^+$. To make CS soluble in a broader pH range, it is modified by covalently linking hydrophilic residues to reactive amino groups.[28] Carboxymethylated and acetylated derivatives, as well as quaternary salts of CS are readily soluble.[29,30] Following the chemical modifications, the solubility of CS was enhanced.

To confirm the galactosylation of CS, the ^{1}H NMR spectra were analyzed for both CS and GC (D2O/AVIII, 300 MHz) (Figure 1, *A* and *B*). The detailed peak assignments in the ^{1}H NMR spectra are shown as follows: CS, δ (ppm): 2.08 (NHCOCH3), 3.18 (H2), 3.38-4.16 (H3-6), 4.62 (H1); GC, δ (ppm): 2.08 (NHCOCH3), 3.01 (H2), 3.35-4.01 (H3-6, H2'-6', Ha-e), 4.17 (Hc), 4.23 (H1'), and 4.62 (H1). The ^{1}H NMR spectrum of CS displayed characteristic peaks including the peaks of protons on the carbons of CS (at 3.00-4.00 ppm) and a peak of methyl protons from partially acetylated CS (at 2.05 ppm), which are consistent with a previous study.[31] The number of hydrogens in GC at δ 3.3-4.2 was higher than that in CS,

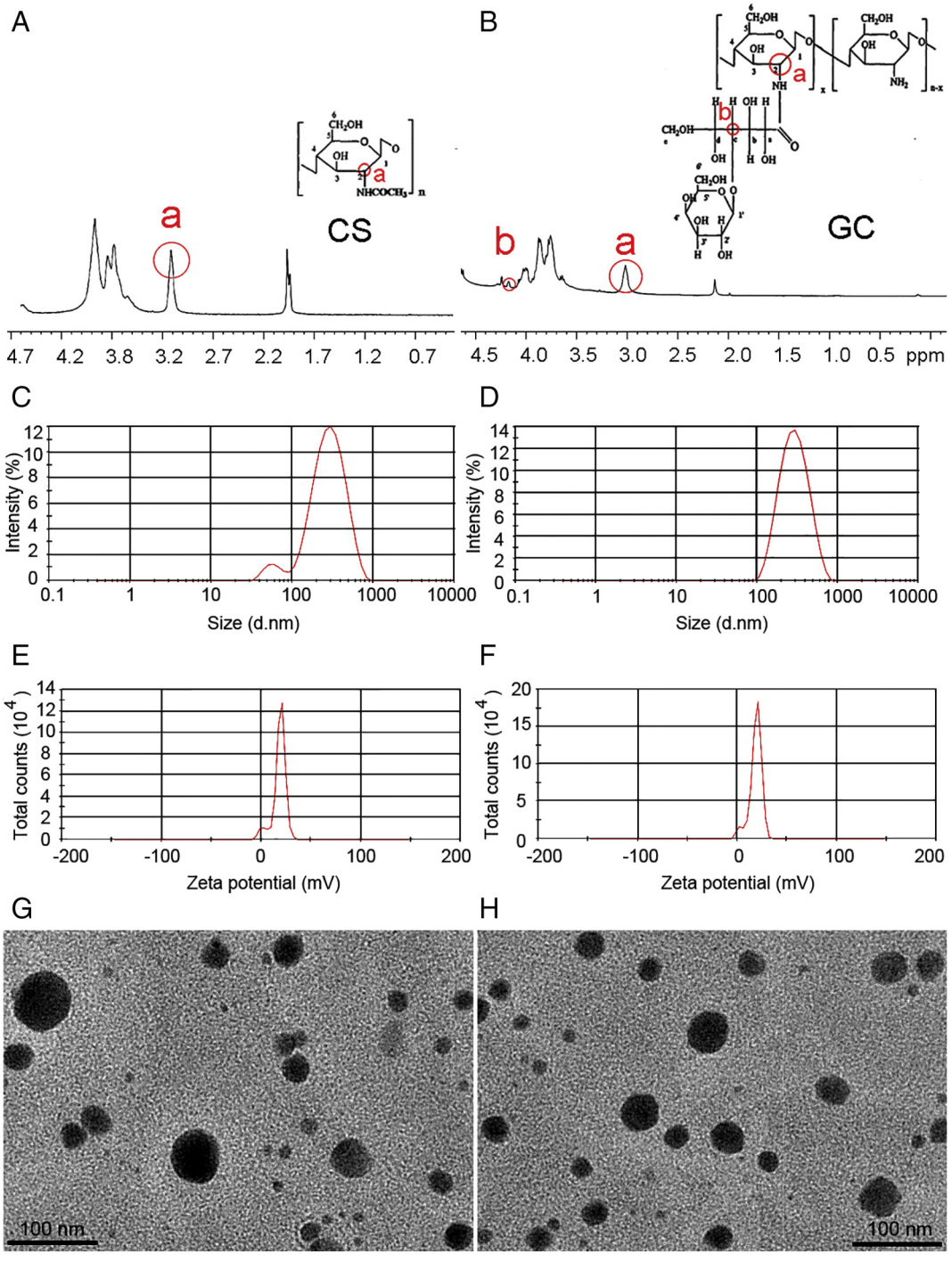

Figure 1. Synthesis of GC and characteristics of the GC-TP-NPs. **(A)** ^{1}H nuclear magnetic resonance spectra of chitosan and **(B)** GC; **(C)** Particle size distribution of pre-lyophilized GC-TP-NPs and **(D)** Lyophilized GC-TP-NPs; **(E)** Zeta potential of pre-lyophilized GC-TP-NPs and **(F)** Lyophilized GC-TP-NPs; **(G)** Transmission electron microscopy images pre-lyophilized GC-TP-NPs and **(H)** Lyophilized GC-TP-NPs.

suggesting that galactose was introduced to CS. The degree of galactose substitution in GC was calculated to be 15.3%.

The particle sizes of the pre-lyophilized and lyophilized GC-TP-NPs were 204.2±1.2 nm and 227.4±3.7 nm, respectively, as determined by TEM (Figure 1, *C* and *D*). The zeta potentials of the corresponding NPs were 18.8±0.5 mV and 19.0±0.3 mV, respectively (Figure 1, *E* and *F*). Both pre-lyophilized and lyophilized GC-TP-NPs showed smooth surface morphologies with near spherical shapes (Figure 1, *G* and *H*). Moreover, EEs of pre-lyophilized and lyophilized GC-TP-NPs were found to be 107.8 ± 6.6% and 88.8 ± 5.9% while LEs were 18.0 ± 1.2% and 14.8 ± 0.9%, respectively. No statistical differences were observed in particle size, zeta potential, morphology, EE and LE between pre-lyophilized and lyophilized GC-TP-NPs, suggesting the NPs had good stability.

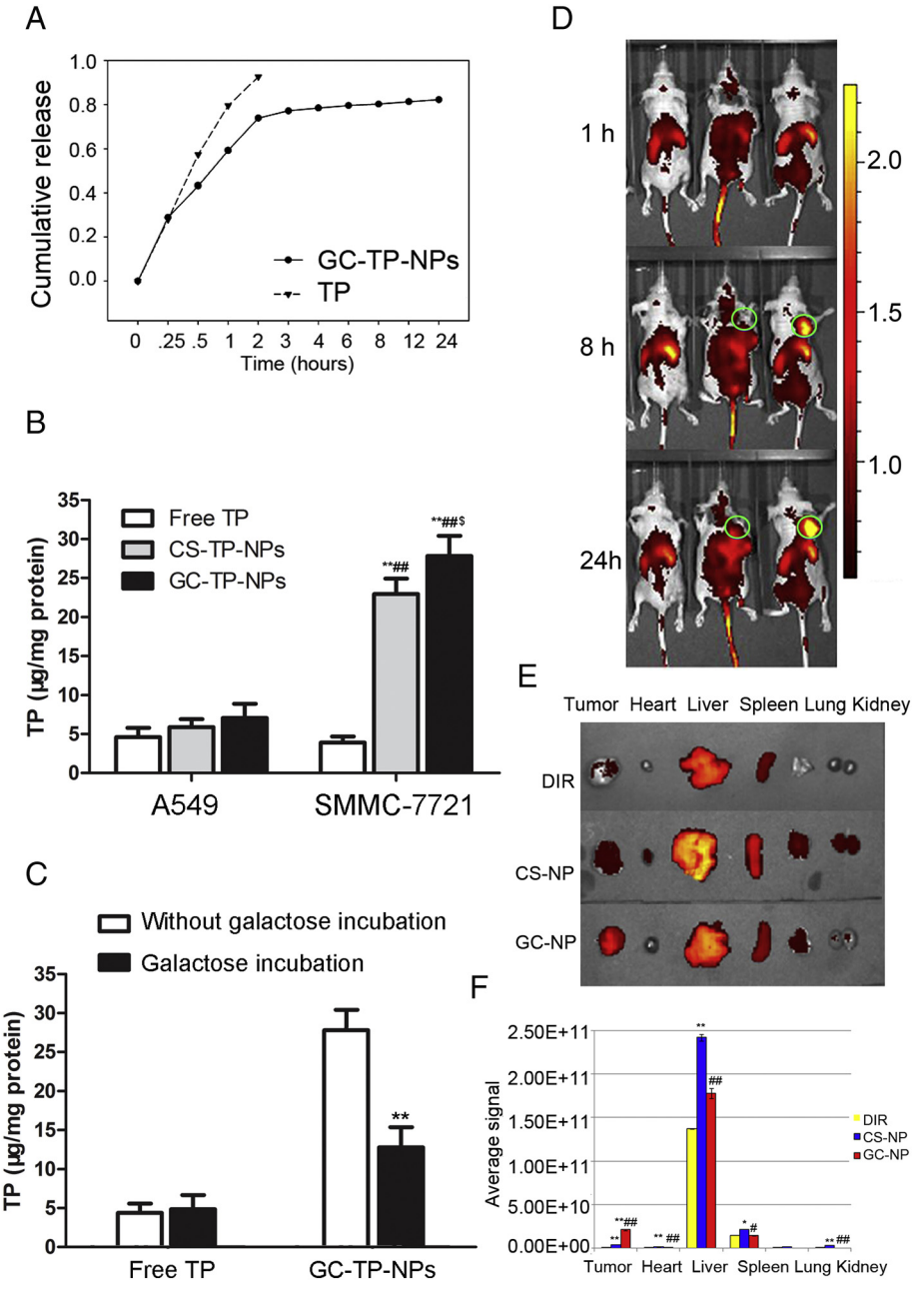

Figure 2. Sustained release profile and cellular uptake of the GC-TP-NPs *in vitro* and hepatoma targeting property of the GC-TP-NPs *in vivo*. **(A)** *In vitro* drug release profiles of the free TP and the GC-TP-NPs. **(B)** The TP content was taken by SMMC-7721 and A549 cells from different TP preparations at a dose of 50 μg/ml TP for 2 h (The data are shown as mean ± SD. $^{**}P < 0.01$, compared with the free TP group; $^{\$}P<0.05$, compared with CS-TP-NPs in the same cell group; $^{\#\#}P < 0.01$, compared with A549 cells treated with the same TP preparations). **(C)** Galactose incubation cell uptake of the free TP and GC-TP-NPs by SMMC-7721 cells (The data are shown as mean ± SD. $^{**}P < 0.01$, compared with the SMMC-7721 cells without galactose incubation). **(D)** DIR fluorescence images of nude mice at different time points. The tumors were marked with green circles. **(E)** DIR fluorescence images of major organs and tumors 24 h after the administration of free DIR-780, DIR-780-loaded-CS-NPs and DIR-780-loaded-GC-NPs. **(F)** Semi-quantitative biodistribution of free DIR-780, DIR-780-loaded-CS-NPs and DIR-780-loaded-GC-NPs in various tissues of nude mice at 24 h. The data are shown as mean ± SD (n = 3; $^{*}P < 0.05$, $^{**}P < 0.01$, compared with the free DIR-780 group; $^{\#}P < 0.05$, $^{\#\#}P < 0.01$, compared with the DIR-780-loaded-CS-NP group).

Sustained release profile of the GC-TP-NPs in vitro

As shown in Figure 2, *A*, free TP and GC-TP-NPs both exhibited a burst release of TP at the initial stage. Specifically, approximately 30.0% of TP was released from both formulations during the first 0.25 h. From then on, free TP continued to be released rapidly and almost completely released within 2 h. In contrast, GC-TP-NPs only released about 70.0% in 2 h. After 24 h of incubation, nearly 80.0% of TP was released from GC-TP-NPs. TP release from GC-TP-NPs was markedly restrained, indicating that GC-TP-NPs may display a sustained release pattern *in vitro*.

ASGP-R mediated cellular uptake of GC-NPs in vitro

The TP content taken up by SMMC-7721 and A549 cells from free TP, CS-TP-NPs, and GC-TP-NPs, was measured, respectively. As shown in Figure 2, *B*, TP entrapped into GC-TP-NPs was taken up more into the SMMC-7721 cells than free TP and CS-TP-NPs (both $P<0.05$). However, there were no significant differences between GC-TP-NPs and free TP, as well as GC-TP-NPs and CS-TP-NPs taken up by A549 cells.

To further verify the influence of ASGP-R mediated endocytosis, the galactose solution was added into SMMC-7721 cells with ASPGR receptor binding sites pre-saturated for competitive inhibition. As shown in Figure 2, *C*, there was no significant difference in the cellular uptake of TP compared to galactose saturated TP under the same conditions. Nevertheless, a distinct difference was observed between galactose incubation and without galactose incubation in GC-TP-NP groups ($P<0.01$). After the pretreatment of galactose, the cellular uptake of the GC-TP-NPs decreased by ~60% compared to that of the control group (setting as 100%).

The above data imply that GC-TP-NPs may function as a grafted galactosyl which specifically recognize ASGP-R on the surface of SMMC-7721 cells, and accelerate its uptake by ASGP-R mediated endocytosis.

Hepatoma targeting property of GC-NPs in vivo

To determine the tumor targeting ability of GC-NPs *in vivo*, a HCC xenograft mouse model was established using SMMC-7721 cells. DIR-780 was used as a fluorescent probe here to investigate the bio-distribution of NPs. At 8 h and 24 h post-injection, the fluorescence signal of DIR-780 was detected to determine the localization of DIR-780-loaded-CS-NPs and DIR-780-loaded-GC-NPs (Figure 2, *D*). After 24 h, a significantly higher accumulation of GC-NPs was found in the liver tumor tissues compared to the CS-NPs and free DIR-780 (Figure 2, *E* and *F*). Although CS-NPs also showed some tumor accumulation due to the local EPR effect of NPs in the inflamed tumor tissue, the signal intensity of CS-NPs in the tumor tissues was much lower than that of GC-NPs (Figure 2, *E* and *F*).

GC-TP-NPs reduced TP-induced hepatic, renal and male reproductive toxicities in vivo

To evaluate the toxicities of the GC-TP-NPs on the liver and kidney, the liver and kidney indexes of Kunming mice treated with free TP or GC-TP-NPs were determined. The liver index of the free TP-treated mice was significantly lower than that of normal mice at both low and high doses (for 1 mg/kg: $P<0.05$; for 2.5 mg/kg: $P<0.01$). On the other hand, the administration of the GC-TP-NPs did not significantly reduce the liver index compared to the normal mice and the liver index was significantly higher than that of the free TP group (for 2.5 mg/kg: $P<0.01$, Figure 3, *A*). In addition, treatment of the free TP tended to decrease the kidney index, although this change was not statistically significant. No changes in the kidney index were observed between the normal and GC-TP-NP groups. To further evaluate the changes of hepatic and kidney function, the serum levels of ALT, AST, Cr and BUN were measured. Significant increases in ALT, AST and Cr levels were observed in mice serum treated with 1 mg/kg of the free TP compared to normal mice ($P<0.01$, Figure 3, *B*). In contrast, the administration of the GC-TP-NPs did not induce significant changes in the levels of those markers (all $P>0.05$, Figure 3, *B*). Additionally, there were no significant differences in the levels of BUN among all groups. Histopathologically, the liver tissues of mice treated with the free TP showed serious cell swelling, vacuolar degeneration and focal necrosis, which correlated well with the significant increases in the liver marker enzymes AST and ALT (Figure 3, *C*). Similarly, significant abnormal alterations were observed in the glomerulus and renal tubes of the free TP-treated mice. In contrast, the administration of the GC-TP-NPs led to a low to moderate degree of histopathological changes in liver tissues. The histopathological changes of the kidney tissues in the GC-TP-NP treatment groups were also smaller than those in the free TP treatment groups at similar TP doses (Figure 3, *C*).

Regarding male reproductive toxicity, the indexes of testes and epididymis significantly decreased after the free TP exposure. In addition, the free TP significantly reduced the levels of testosterone, glutathione peroxidase (GSH-PX) and α-glucosidase in testes compared to controls ($P<0.01$). When treated with the GC-TP-NPs, testicular and epididymal indexes were similar to the control group but were significantly higher than the free TP-treated group (Figure 3, *D*). Additionally, the concentrations of testosterone, GSH-PX and α-glucosidase in the GC-TP-NP-treated groups were significantly higher than those in the TP-treated groups ($P<0.05$), but had no significant difference compared to the control group ($P>0.05$, Figure 3, *E*). Histopathologically, testicular sections of the free TP-treated mice showed severe degenerative changes characterized by disorganized seminiferous tubules indicating impaired spermatogenesis. An increased number of sloughing tubules containing necrotic germ cells, and a loss of elongated spermatids and spermatozoa were also observed in most of the seminiferous tubules. Contrarily, the testicular structures in both the control and GC-TP-NP-treated groups were normal without significant pathological changes. The epididymis sections in the free TP-treated groups showed a significant decrease of mature spermatozoa concentration in the lumen and interstitial edema, which was not found in the GC-TP-NP-treated groups (Figure 3, *F*). Finally, the free TP treatment in males led to a significant decrease in sperm count, density, motility and viability compared to the control group ($P<0.01$, Supplementary Table S4). The treatment with the GC-TP-NPs minimized the toxic effects of TP and significantly improved semen quality ($P<0.01$, Supplementary Table S4), although none of the parameters reached the levels observed in the control mice.

GC-TP-NPs inhibited cell proliferation and induced HCC cell apoptosis

Cells were treated with the free TP and GC-TP-NPs at 0.01, 0.1, 0.5, 2.5, 5, 10 and 50 μg/mL of equivalent TP concentrations for 24 (Figure 4, *A*) and 48 h (Figure 4, *B*). The results demonstrated that the growth of HepG2 cells was significantly inhibited by the treatment of the free TP and GC-TP-NPs. The IC50 values of the free TP and GC-TP-NPs against HepG2 cells

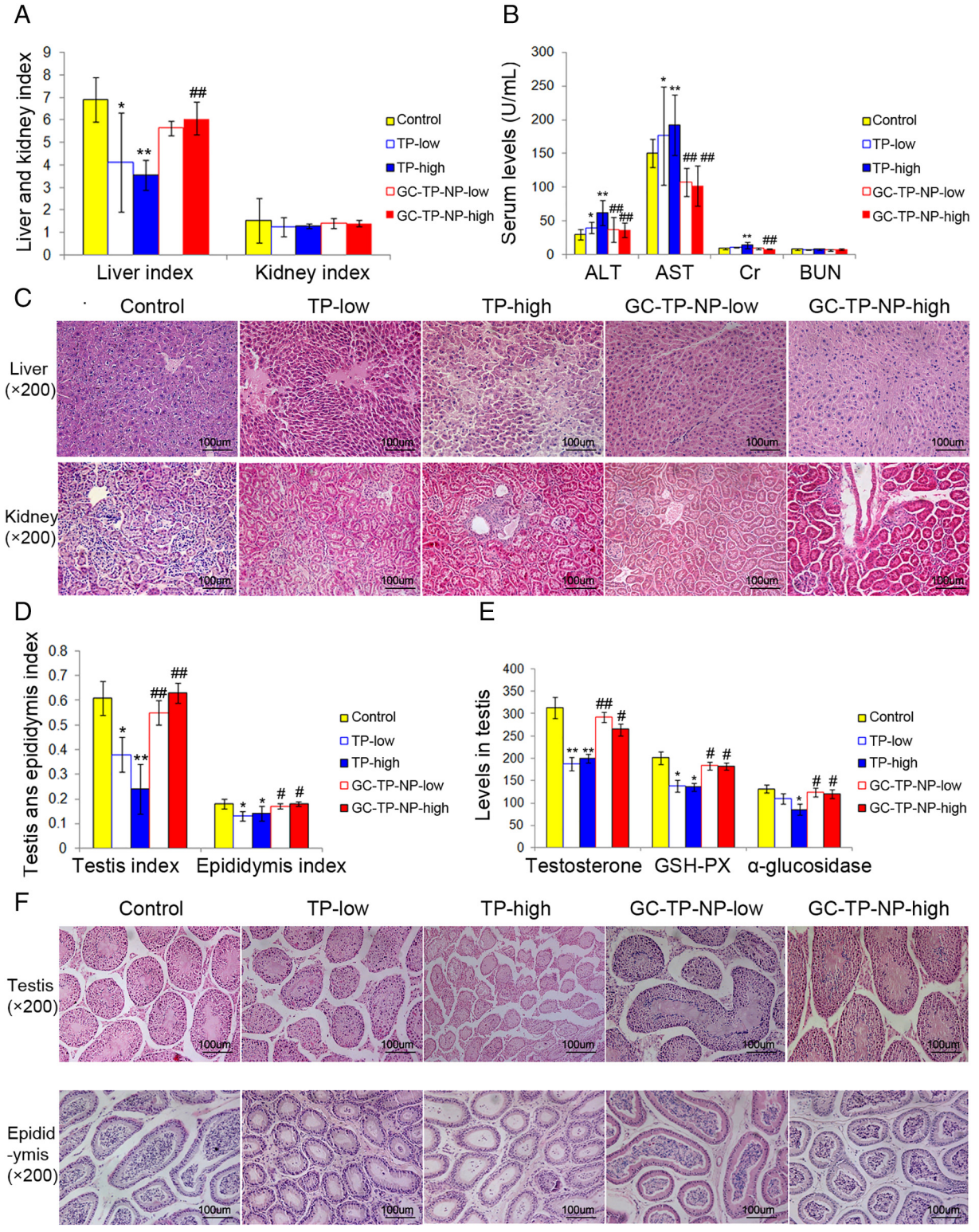

Figure 3. GC-TP-NPs reduce TP-induced hepatic and renal toxicities, as well as male reproductive toxicity *in vivo*. **(A)** Liver and kidney index of mice in different groups; **(B)** Serum levels of ALT, AST, Cr and BUN in different groups; **(C)** Histopathological changes in liver and kidney tissues of different groups; **(D)** Testis and epididymis index of mice in different groups; **(E)** Testosterone, GSH-PX and α-glucosidase levels in testes from different groups; **(F)** Histopathological changes in testis and epididymis tissues from different groups. The data are shown as mean ± SD (*$P < 0.05$, **$P < 0.01$, compared with the control group; $^{\#}P < 0.05$, $^{\#\#}P < 0.01$, TP-low vs. GC-TP-NP-low or TP-high vs. GC-TP-NP-high).

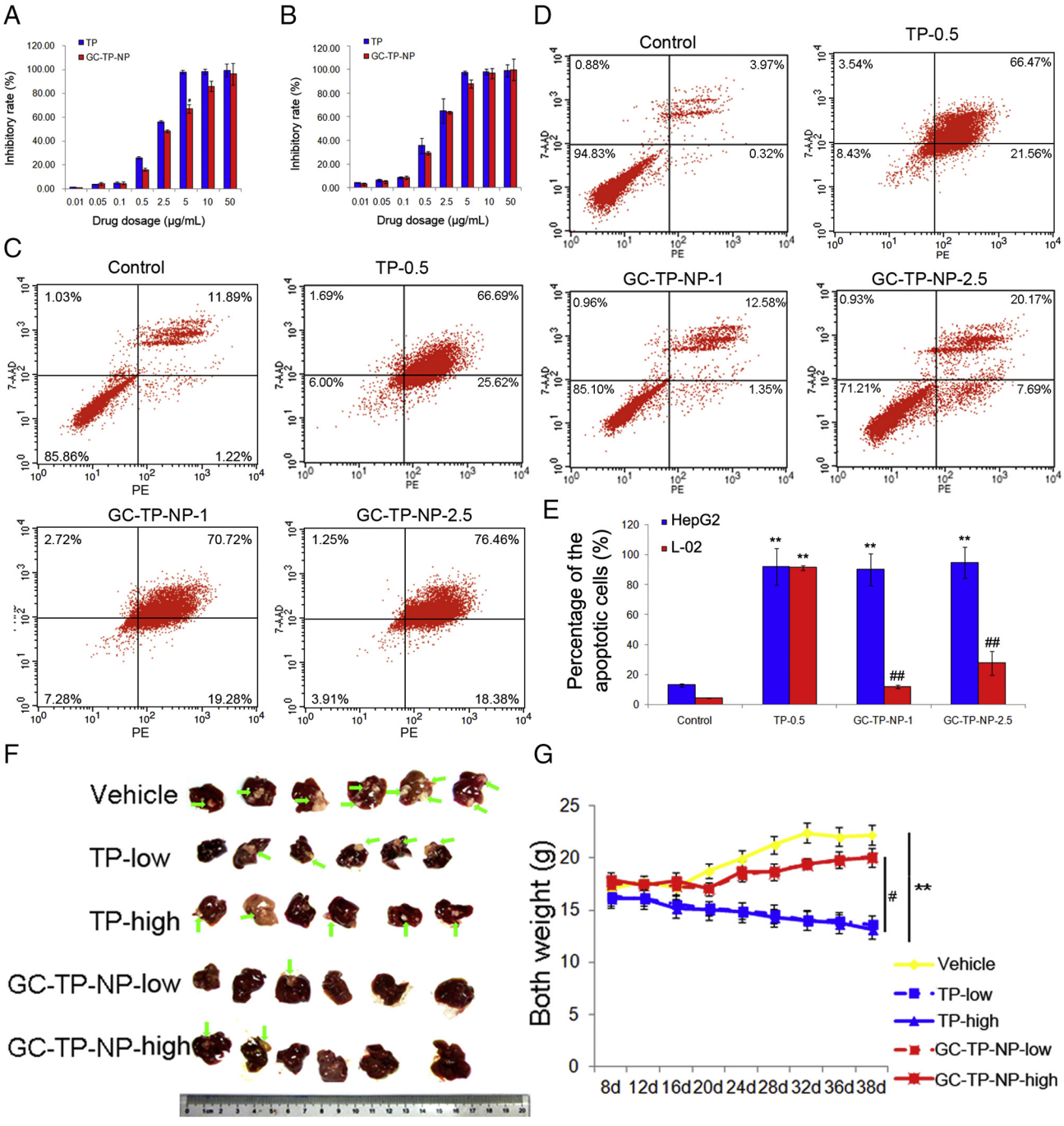

Figure 4. Anti-HCC activities of the GC-TP-NPs *in vitro* and *in vivo*. **(A** and **B)** Inhibitory rates of the free TP and GC-TP-NPs to HepG2 cells at 24 h and 48 h, respectively. **(C** and **D)** Cell apoptosis levels in the control, free-TP-0.5, GC-TP-NP-1 and GC-TP-NP-2.5 groups based on HepG2 and L-02 cells, respectively. The fluorescence intensity of apoptotic cells is expressed as channel numbers in quadrants of each plots; the cells in top right and bottom right quadrants are in early and late apoptosis, respectively. **(E)** Percentage of apoptotic cells in different groups shown in **(D)**. **(F)** Representative tumor-bearing livers in mice at the therapeutic end point of different groups. Tumor tissues were marked with the green arrows. **(G)** Average mouse body weight for the different treatment groups. The data are shown as mean ± SD. $^{**}P<0.01$, compared with the control group; $^{***}P<0.001$, compared with the control group; $^{\#}P<0.05$, compared with the free TP-treated group (GC-TP-NP-low vs. TP-low or GC-TP-NP-high vs. TP-high).

had no significant difference when treated for 24 h (free-TP vs. GC-TP-NPs: 1.61±0.69 vs. 2.08±0.53; $P>0.05$) and for 48 h (free-TP vs. GC-TP-NPs: 0.90±0.46 vs. 1.14±0.48; $P>0.05$).

Flow cytometry analysis was performed to investigate the effects of the free TP and GC-TP-NPs on HepG2 and L-02 cell apoptosis. The percentages of the apoptotic HepG2 cells treated with the free TP (0.5 μg/mL) and GC-TP-NPs (2.5 μg/mL) were 92.31±12.09% and 94.85±10.49%, respectively, which were both significantly higher than the cells without any treatment (13.11±1.16%, both $P<0.01$, Figure 4, *C* and *E*). However, the

difference between the free TP and GC-TP-NP groups had no statistical significance. More importantly, the percentages of apoptotic L-02 cells treated with GC-TP-NPs (1.0 μg/mL and 2.5 μg/mL) were both significantly lower than that of apoptotic HepG2 cells treated with the same treatment (13.93±1.16% vs. 90.00±10.68% and 27.86±7.85% vs. 94.85±10.49%, both $P<0.01$, Figure 4, *D* and *E*), suggesting that the GC-TP-NPs might induce HCC cell apoptosis more obviously than normal liver cells.

GC-TP-NPs reduced tumor burden in orthotopic mouse models

To evaluate the *in vivo* anti-cancer efficacy of the GC-TP-NPs, an orthotopic HCC model was established. This model was selected as it is a natural representative of a native tumor due to the growth of tumor cells in the liver. Compared to the free TP treatment groups, liver tumor sizes of mice treated with the GC-TP-NPs were significantly smaller, and the high dosage of the GC-TP-NPs showed the greatest efficacy (Figure 4, *F*). Although there were also decreases in the tumor sizes when treated with high TP, cirrhosis and size decreases were observed in these liver tissues. Contrarily, there was no marked change in liver tissues in the GC-TP-NP treatment groups. In addition, compared to the control group, the GC-TP-NP-treated mice showed stable body weights similar to the control group ($P>0.05$), whereas the treatment with the free TP resulted in significant weight loss ($P<0.05$, Figure 4, *G*), which indicated significant toxicity of the free TP.

GC-TP-NPs induced HCC cell apoptosis via blocking TNF/NF-κB/BCL2 signaling

To further investigate the pharmacological mechanisms of the free TP and GC-TP-NPs against HCC, a list of TP putative targets was first predicted based on the chemical constituents' structural similarity (Supplementary Table S1) and HCC-related genes were collected from the existing gene–gene interaction databases according to our previous studies[24,25] (Supplementary Table S2). A "drug target–disease gene interaction network" was constructed using the interactions among TP putative targets and HCC-related genes. Next, a sub-network containing 133 direct interactions between 10 TP putative targets and 48 HCC-related genes was constructed and functionally associated with apoptosis signaling, MAPK signaling, and several inflammatory response pathways, such as T/B cell receptor signaling, NOD-like receptor signaling, Fc epsilon RI signaling, and Toll-like receptor signaling (Figure 5, *A*). Among these genes, most TP putative targets, such as tumor necrosis factor (*TNF*), nuclear factor kappa B subunit 1 (*NFKB1*), NFKB inhibitor alpha (*NFKBIA*), RELA proto-oncogene, NF-kB subunit (*RELA*), BCL2, apoptosis regulator (*BCL2*), and X-linked inhibitor of apoptosis (*XIAP*), were involved in apoptosis signaling, implying the potential role of TP in this pathway.

Apoptosis plays crucial roles in tissue homeostasis, immunity and embryological development.[32] The apoptotic pathway initiates with the formation of a complex between tumor necrosis factor-α (TNF-α) and its receptor (TNFR) on cell surfaces, which leads to interactions between TNFR and TNFRSF1A associated death domain (TRADD) (Figure 5, *B*). Following the interaction between TRADD, the TNF Receptor Associated Factor-2 (TRAF2), and the kinase RIP1 (Receptor-Interacting Protein-1), NF-kB signaling may be activated. Activation of NF-KB, NFKB1 (p50), NFKB1A and RELA (p65) is associated with upregulation of the anti-apoptotic BCL2 protein and IAPs (Inhibitor of Apoptosis Proteins), resulting in cell survival.[33] In addition, TNF-α can trigger both anti-apoptotic NF-kB signaling and apoptosis signaling simultaneously.[34,35] Herein, an agent may potentiate TNF-α-induced apoptosis by inhibiting TNF-α-induced anti-apoptotic NF-kB signaling.[36] Therefore, we hypothesized that TP may induce tumor cell apoptosis via inhibiting candidate targets including TNF, NFKB1, NFKB1A, RELA, BCL2 and XIAP, which are all involved in TNF-α-induced anti-apoptotic NF-kB signaling as mentioned above.

To experimentally validate the above hypothesis, western blot analysis was performed. Results showed that both the free TP and GC-TP-NPs efficiently inhibited the expression of TNF, NFKB1, NFKB1A, RELA, BCL2 and XIAP proteins in liver tumor tissues when compared to the vehicle only group (Figure 5, C, $P<0.05$). Notably, the inhibitory effects of the GC-TP-NPs treatment on the target proteins were significantly higher than that of the free TP treatments (GC-TP-NP-high vs. TP-high; $P<0.05$).

Discussion

HCC has an unfavorable prognosis due to its poor response to current therapeutic strategies. TP has been suggested to be more potent against HCC than other therapeutic agents such as doxorubicin, daunorubicin and sorafenib.[37] However, its clinical application is limited due to its poor solubility and high toxicity.[11] Therefore, it is of great importance to improve its therapeutic index and reduce the side effects of TP in the treatment of HCC. Growing evidence shows that NP-based targeted delivery systems can aid in enriching drug concentration at target sites while minimizing systemic exposure.[15,16] In the current study, GC-TP-NPs with a near spherical shape, small particle diameters (~200 nm) and high drug loading capacity (~90%) were successfully synthesized. Consistent with previous findings,[38,39] our data demonstrated that although it suppressed HCC progression, the free TP caused significant toxicity. Contrarily, the GC-TP-NPs displayed a stronger anti-cancer efficacy and lower systemic toxicity on orthotopic xenograft HCC models than the free TP. To elucidate the pharmacological mechanisms of TP against cancer, a network pharmacology-based investigation was performed in this study. Results indicated that the free TP and GC-TP-NPs may exert their anti-HCC activities through regulating target genes involved in apoptosis signaling including *TNF, NFKB1, NFKB1A, RELA, BCL2* and *XIAP*.

In addition, our data demonstrated a stronger *in vivo* anti-HCC efficacy of the GC-TP-NPs than the free TP. This increased efficacy is likely due to several advantages of the GC-TP-NPs. First, an efficient hepatoma-targeting was observed by the GC-TP-NPs, most likely due to the addition of galactose groups that are specific adhesive ligands to ASGP-R on the surface of HCC cells. In the current study, we found that the GC-TP-NPs were

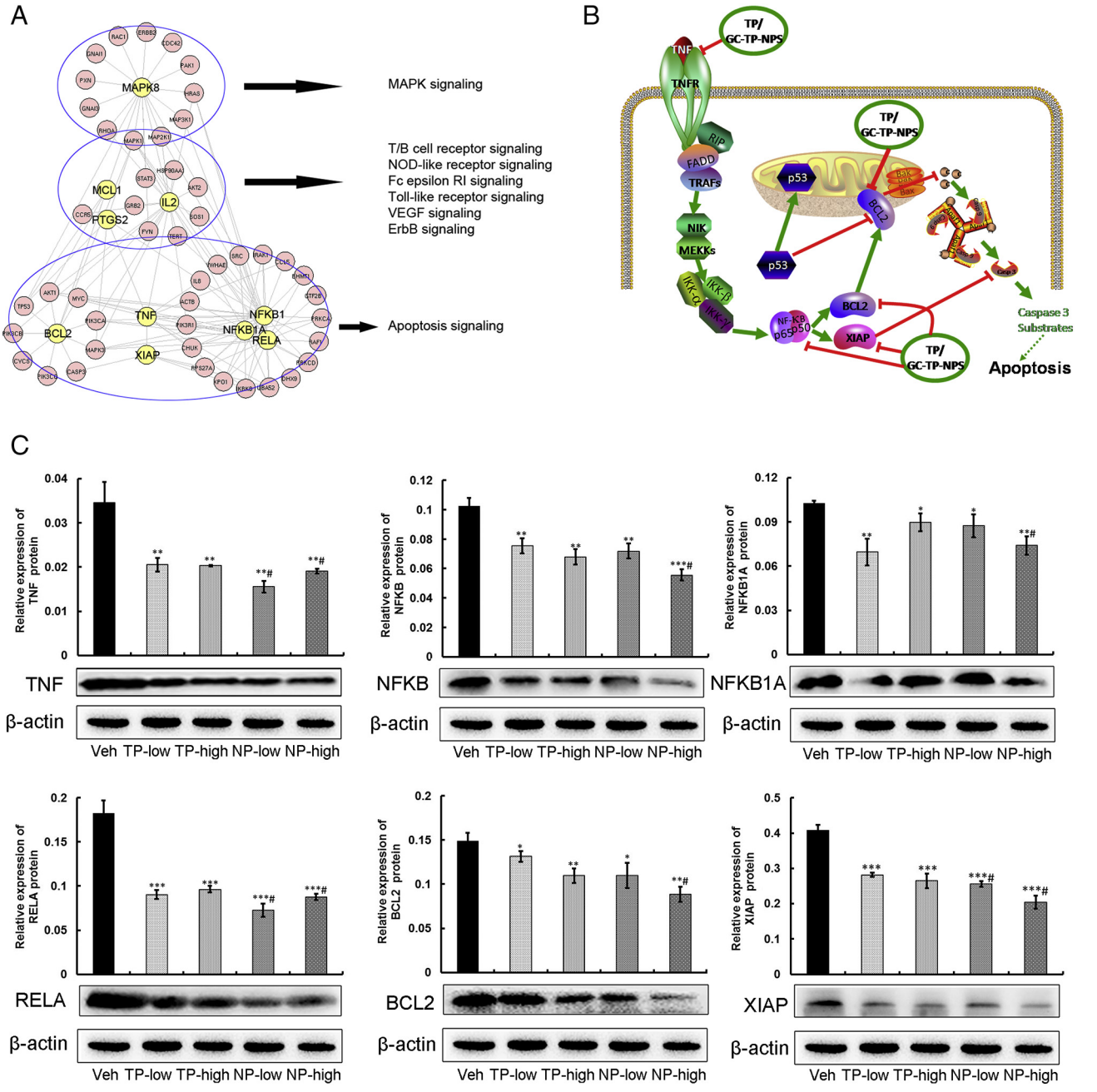

Figure 5. Network pharmacology-based investigation and experimental validations on the mechanisms of TP/GC-TP-NPs acting on HCC. **(A)** Sub-network of TP putative target (yellow nodes)-HCC-related gene (pink nodes) direct interactions, and the signal pathways involved by the functional modules. **(B)** Illustrations of apoptosis signaling involved by most of TP putative targets. **(C)** Expression levels of TNF, NFKB1, NFKB1A, RELA, BCL2 and XIAP proteins in different groups detected by Western blot analyses. Data are represented as the mean ± SEM (n=6). * P<0.05, ** P<0.01, and *** P<0.001 versus the vehicle group, respectively. # P<0.05 versus the free TP group (GC-TP-NP-low vs. TP-low or GC-TP-NP-high vs. TP-high).

taken up more into the SMMC-7721 cells with high expression levels of ASGP-R than A549 cells without ASGP-R expression, and also revealed that exogenous galactose competitively inhibited HCC cell uptake of the GC-TP-NPs, indicating the ASGP-R mediated endocytosis of the GC-TP-NPs. Second, the GC-TP-NPs may accumulate more at the tumor site through the EPR effect, as compared to normal tissues, leading to a stronger tumor inhibition. Third, the release of the TP from the GC-TP-NPs occurred in a sustained manner, which may help to maintain higher TP concentrations for longer periods at the diseased sites compared to the free TP. Fourth, the systemic toxicity of TP was significantly alleviated following its encapsulation in NPs. Finally, the GC-TP-NPs have positively charged surfaces, which may facilitate NP binding to the negatively charged tumor cell surfaces, leading to more TP-containing NPs entering tumor cells and exerting anti-tumor effects.

Despite the potential of TP as an anti-cancer drug, previous attempts to clarify its mechanisms of action have not been successful. Network pharmacology-based approaches, which integrate drug target prediction, drug-disease network analysis and key network target screening, have been demonstrated as efficient methods to investigate the mechanism of action for a drug, especially for plant-derived drugs.[40,41] Herein, a TP target-HCC-related gene interaction network was constructed followed by the prediction of TP targets. Functionally, TP putative targets, which directly interacted with HCC-related genes, were found to be mostly associated with apoptosis signaling pathways, implying that TP may kill hepatoma cells via induced apoptosis, which is in agreement with previous reports.[42–44] Specifically, we identified six TP putative targets, including TNF, NFKB1, NFKBIA, RELA, BCL2 and XIAP, which are crucial components in the apoptosis signaling pathway (Figure 5, *B*). Our results demonstrated that the administration of both the free TP and GC-TP-NPs efficiently reduced the expression levels of TNF, NFKB1, NFKBIA, RELA, BCL2 and XIAP proteins in hepatoma tissues. More interestingly, our data further demonstrated a stronger target regulation efficacy of the GC-TP-NPs compared to the free drug.

In conclusion, our data demonstrated that the anti-HCC activities of the free TP were at a cost of serious toxicity. Conversely, the GC-TP-NPs can prevent cancer progression with an increase in efficacy while mitigating systemic toxicity due to hepatocyte-targeted delivery and a sustained TP release profile. More importantly, we also revealed that the GC-TP-NPs may inhibit HCC by inducing cancer cell apoptosis via blocking TNF/NF-κB/BCL2 signaling. Thus, the GC-TP-NP may be a potentially biocompatible and eligible candidate drug for HCC therapy.

Authors' contribution

Prof. Yanqiong Zhang, Prof. Thomas J. Webster and Prof. Na Lin conceived the study, participated in its design and coordination, and helped to draft the manuscript. Prof. Yanqiong Zhang and Prof. Yan Shen carried out the experiments and drafted the manuscript. The other authors participated in the design of the study and performed the statistical analyses. All authors read and approved the final manuscript.

Appendix A. Supplementary data

Supplementary data to this article can be found online at https://doi.org/10.1016/j.nano.2018.09.002.

References

1. Dimitroulis D, Damaskos C, Valsami S, Davakis S, Garmpis N, Spartalis E. From diagnosis to treatment of hepatocellular carcinoma: An epidemic problem for both developed and developing world. *Gastroenterol* 2017;**23**:5282-94.
2. Khemlina G, Ikeda S, Kurzrock R. The biology of hepatocellular carcinoma: implications for genomic and immune therapies. *Mol Cancer* 2017;**16**:149.
3. Cidon EU. Systemic treatment of hepatocellular carcinoma: Past, present and future. *Hepatol* 2017;**9**:797-807.
4. Montella L, Palmieri G, Addeo R, Del Prete S. Hepatocellular carcinoma: Will novel targeted drugs really impact the next future? *Gastroenterol* 2016;**22**:6114-26.
5. Mao J, Liu S, Ai M, Wang Z, Wang D, Li X. A novel melittinnano-liposome exerted excellent anti-hepatocellular carcinoma efficacy with better biological safety. *J Hematol Oncol* 2017;**10**:71.
6. Badrealam KF, Owais M. Nano-Sized drug delivery systems: development and implication in treatment of hepatocellular carcinoma. *Dig Dis* 2015;**33**:675-82.
7. Ziaei S, Halaby R. Immunosuppressive, anti-inflammatory and anti-cancer properties of triptolide: a mini review. *Phytomed* 2016;**6**:149-64.
8. Gali-Muhtasib H, Hmadi R, Kareh M, Tohme R, Darwiche N. Cell death mechanisms of plant-derived anticancer drugs: beyond apoptosis. *Apoptosis* 2015;**20**:1531-62.
9. Chan EW, Cheng SC, Sin FW, Xie Y. Triptolide induced cytotoxic effects on human promyelocytic leukemia, T cell lymphoma and human hepatocellular carcinoma cell lines. *Toxicol Lett* 2001;**122**:81-7.
10. Alsaied OA, Sangwan V, Banerjee S, Krosch TC, Chugh R, Saluja A. Sorafenib and triptolide as combination therapy for hepatocellular carcinoma. *Surgery* 2014;**156**:270-9.
11. Ling D, Xia H, Park W, Hackett MJ, Song C, Na K. pH-sensitive nanoformulatedtriptolide as a targeted therapeutic strategy for hepatocellular carcinoma. *ACS Nano* 2014;**8**:8027-39.
12. Banerjee S, Saluja A. Minnelide, a novel drug for pancreatic and liver cancer. *Pancreatology* 2015;**15**(4 Suppl):S39-43.
13. Mohamed NK, Hamad MA, Hafez MZ, Wooley KL, Elsabahy M. Nanomedicine in management of hepatocellular carcinoma: challenges and opportunities. *Cancer* 2017;**140**:1475-84.
14. Liang S, Xu S, Zhang D, He J, Chu M. Reproductive toxicity of nanoscalegraphene oxide in male mice. *Nanotoxicology* 2015;**9**:92-105.
15. Wakaskar RR. Promising effects of nanomedicine in cancer drug delivery. *J Drug Target* 2017:1-24.
16. Wicki A, Witzigmann D, Balasubramanian V, Huwyler J. Nanomedicine in cancer therapy: challenges, opportunities, and clinical applications. *J Control Release* 2015;**200**:138-57.
17. Yu RS, Zhu XL, Sun JZ, Shi D, Chen Y, Wang ZK. Preliminary study on hepatocyte-targeted phosphorus-31 MRS using ATP-loaded galactosylated chitosan oligosaccharide nanoparticles. *Gastroenterol Res Pract* 2013;**2013**:512483.
18. Huang C, Li NM, Gao P, Yang S, Ning Q, Huang W. In vitro and in vivo evaluation of macromolecular prodrug GC-FUA based nanoparticle for hepatocellular carcinoma chemotherapy. *Drug Deliv* 2017;**24**:459-66.
19. Wang D, Chang R, Wang G, Hu B, Qiang Y, Chen Z. Polo-like kinase 1-targeting chitosan nanoparticles suppress the progression of hepatocellular carcinoma. *Anticancer Agents Med Chem* 2017;**17**:948-54.
20. Yu JM, Li WD, Lu L, Zhou XY, Wang DY, Li HM. Preparation and characterization of galactosylated glycol chitosan micelles and its potential use for hepatoma-targeting delivery of doxorubicin. *J Mater Sci Mater Med* 2014;**25**:691-701.
21. Zhu XL, Du YZ, Yu RS, Liu P, Shi D, Chen Y. Galactosylated chitosan oligosaccharide nanoparticles for hepatocellular carcinoma cell-targeted delivery of adenosine triphosphate. *MolSci* 2013;**14**:15755-66.
22. Zhou N, Zan X, Wang Z, Wu H, Yin D, Liao C. Galactosylated chitosan-polycaprolactone nanoparticles for hepatocyte-targeted delivery of curcumin. *Carbohydr Polym* 2013;**94**:420-9.
23. Wang Q, Zhang L, Hu W, Hu ZH, Bei YY, Xu JY, et al. Norcantharidin-associated galactosylated chitosan nanoparticles for hepatocyte-targeted delivery. *Nanomedicine* 2010;**6**:371-81.
24. Zhang Y, Li Z, Yang M, Wang D, Yu L, Guo C. Identification of GRB2 and GAB1 coexpression as an unfavorable prognostic factor for hepatocellular carcinoma by a combination of expression profile and network analysis. *PLoS ONE* 2013;**2013**:8.
25. Zhang Y, Guo X, Yang M, Yu L, Li Z, Lin N. Identification of AKT kinases as unfavorable prognostic factors for hepatocellular carcinoma

by a combination of expression profile, interaction network analysis and clinical validation. *Mol Biosyst* 2014;**2014**:10.
26. Zhang Y, Guo X, Xiong L, Kong X, Xu Y, Liu C. MicroRNA-101 suppresses SOX9-dependent tumorigenicity and promotes favorable prognosis of human hepatocellular carcinoma. *FEBS Lett* 2012;**586**:4362-70.
27. Zhang Y, Guo X, Xiong L, Yu L, Li Z, Guo Q. Comprehensive analysis of microRNA-regulated protein interaction network reveals the tumor suppressive role of microRNA-149 in human hepatocellular carcinoma via targeting AKT-mTOR pathway. *Mol Cancer* 2014;**2014**:13.
28. Il'ina AV, Varlamov VP. Galactosylated derivatives of low-molecular-weight chitosan: production and properties. *Prikl Biokhim Mikrobiol* 2007;**43**:82-7.
29. Kato Y, Onishi H, Machida Y. Application of chitin and chitosan derivatives in the pharmaceutical field. *Curr Pharm Biotechnol* 2003;**4**:303-9.
30. Zou Y, Khor E. Preparation of C-6 substituted chitin derivatives under homogeneous conditions. *Biomacromolecules* 2005;**6**:80-7.
31. Zheng D, Duan C, Zhang D, Jia L, Liu G, Liu Y, et al. Galactosylated chitosan nanoparticles for hepatocyte-targeted delivery of oridonin. *Pharm* 2012;**436**:379-86.
32. Huang L, Chaurasiya B, Wu D, Wang H, Du Y, Tu J, et al. Versatile redox-sensitive pullulan nanoparticles for enhanced liver targeting and efficient cancer therapy. *Nanomedicine* 2018;**14**:1005-17.
33. Cao ZH, Yin WD, Zheng QY, Feng SL, Xu GL, Zhang KQ. Caspase-3 is involved in IFN-γ- and TNF-α-mediated MIN6 cells apoptosis via NF-κB/Bcl-2 pathway. *Cell Biochem Biophys* 2013;**67**:1239-48.
34. Karin M, Cao Y, Greten FR, Li ZW. NF-kappaB in cancer: from innocent bystander to major culprit. *Nat Rev Cancer* 2002;**2**:301-10.
35. Ding WX, Yin XM. Dissection of the multiple mechanisms of TNF-alpha-induced apoptosis in liver injury. *J Cell Mol Med* 2004;**8**:445-54.
36. Shi J, Chen J, Serradji N, Xu X, Zhou H. PMS1077 sensitizes TNF-a induced apoptosis in human prostate cancer cells by blocking NF-kB signaling pathway. *PLoS ONE* 2013;**8**:e61132.
37. Meng C, Zhu H, Song H, Wang Z, Huang G, Li D. Targets and molecular mechanisms of triptolide in cancer therapy. *Cancer Res* 2014;**26**:622-6.
38. Li XJ, Jiang ZZ, Zhang LY. Triptolide: progress on research in pharmacodynamics and toxicology. *J Ethnopharmacol* 2014;**155**:67-79.
39. Li M, Hu T, Tie C, Qu L, Zheng H, Zhang J. Quantitative proteomics and targeted fatty acids analysis reveal the damage of triptolide in liver and kidney. *Proteomics* 2017;**17**:22.
40. Zhang Y, Guo X, Wang D, Li R, Li X, Xu Y. A systems biology-based investigation into the therapeutic effects of GansuiBanxia Tang on reversing the imbalanced network of hepatocellular carcinoma. *Sci Rep* 2014;**4**:4154.
41. Zhang Y, Bai M, Zhang B, Liu C, Guo Q, Sun Y. Uncovering pharmacological mechanisms of Wu-tou decoction acting onrheumatoid arthritis through systems approaches: drug-target prediction, network analysis and experimental validation. *Sci Rep* 2015;**5**:9463.
42. Zhang Y, Mao X, Guo Q, Bai M, Zhang B, Liu C. Pathway of PPAR-gamma coactivators in thermogenesis: a pivotal traditional Chinese medicine-associated target for individualized treatment of rheumatoid arthritis. *Oncotarget* 2016;**7**:15885-900.
43. Wang H, Ma D, Wang C, Zhao S, Liu C. Triptolide inhibits invasion and tumorigenesis of hepatocellular carcinoma MHCC-97H cells through NF-κB signaling. *Med Sci Monit* 2016;**22**:1827-36.
44. Li SG, Shi QW, Yuan LY, Qin LP, Wang Y, Miao YQ, et al. C-Myc-dependent repression of two oncogenic miRNA clusters contributes to triptolide-induced cell death in hepatocellular carcinoma cells. *J Exp Clin Cancer Res* 2018;**37**:51.